ELSEVIER

Journal of Fluorine Chemistry 119 (2003) 173–189

JOURNAL OF FLUORINE CHEMISTRY

www.elsevier.com/locate/jfluchem

Electrochemistry of fluorine production

Henri Groult*

Laboratoire LI2C-CNRS UMR 7612, Université P.&M. Curie, 4 Place Jussieu, 75252 Paris Cedex 05, France

Received 24 July 2002; received in revised form 7 October 2002; accepted 9 October 2002

Abstract

The electronic properties of carbon–fluorine films (denoted C–F) formed on carbon electrodes in KF–2HF during fluorine evolution reaction were investigated in aqueous solution containing a redox couple and in mercury. It was shown that the passivating C–F films behave as electronic conductors. STM measurements have shown composition heterogeneities at the surface of fluorinated HOPG (conducting ans insulating areas). The influence of the amount of insulating graphite fluorides on the surface of the electrodes was demonstrated. Thus, the high anodic overvoltage observed during fluorine evolution on C/C–F anodes in KF–2HF is mainly attributed to the poor wettability of the electrodes by the melt, which results in a small electroactive area. A new model was proposed for representing the electrode/electrolyte interface; it includes the presence of a ''fluidized'' layer between the surface C–F film and the fluorine gas film. The ''fluidized'' layer is composed of liquid KF–2HF melt and dissolved fluorine gas. The influence of the mass transfer phenomenon occurring in that layer was pointed out mainly by impedance measurements. Finally, the contributions of the C–F film, η_{C-F}, and of the ''fluidized'' layer, η_{fluid}, to the total anodic overvoltage, η_T, were studied using a numerical calculation method. Both contributions must be taken into account for a global understanding of the fluorine evolution process.

Keywords: Fluorine; KF–2HF; Anodic overvoltage; Carbon

1. Introduction

Fluorine [1–3] was discovered by the Swedish chemist C.W. Scheele in 1771, but isolated only about one century later in 1886 by the French chemist H. Moissan who performed electrolysis of anhydrous hydrogen fluoride containing a small amount of potassium fluoride. The latter was used to render HF conducting. Fluorine and hydrogen were produced at the anode and the cathode, respectively according to the following global reaction:

$$HF_{(liq.)} \rightarrow F_{2(g)} + H_{2(g)} \quad (1)$$

The two corresponding half-cell reactions are supposed to be:

$$HF_2^- \rightarrow \tfrac{1}{2}F_2 + HF + e^- \quad (2)$$

at the anode, and:

$$2HF + e^- \rightarrow \tfrac{1}{2}H_2 + HF_2^- \quad (3)$$

at the cathode.

Nowadays, most of elemental fluorine production is involved in the manufacture of hexafluorides of uranium (UF_6) and sulfur (SF_6). Therefore, F_2 is a necessary intermediate in uranium isotopic concentration: separation of the isotopes of natural uranium is carried out by a diffusion process involving gaseous UF_6. Uranium tetrafluoride (UF_4) is first produced by the reaction of UO_2 and HF. UF_6 is then prepared exclusively by the action of fluorine gas and UF_4 according to:

$$UF_4 + F_2 \rightarrow UF_6 \quad (4)$$

Because of the reactivity of elemental fluorine, special care must be taken in holding and storing this gas. Nevertheless, elemental fluorine is more and more used for the preparation of several products such as fluorochemicals, WF_6 (CVD), NF_3 for etching of semiconductors, graphite fluorides as cathodes in primary lithium batteries and as lubricating agent, solid fluorine carriers (CoF_3, ...) and so on.

A typical industrial cell operates at 6 kA and contains molten KF–2HF (40.8 wt.% HF) with about 30 plate carbon anodes and steel or iron cathodes. Indeed, because of anodic dissolution of most metals which may occur in parallel with the evolution of fluorine, only carbon anodes are used. Non-graphitized carbon anodes are suitable but graphite anodes

* Tel.: +33-1-44-27-35-34; fax: +33-1-44-27-38-56.
E-mail address: groult@ccr.jussieu.fr (H. Groult).

0022-1139/02/$ – see front matter
PII: S0022-1139(02)00252-X

are not since exfoilation takes place during intercalation of the constituents of the melt between the lamellar graphene layers. The cells are also equipped with monel skirts to separate the gases in order to avoid explosive recombination.

The fluorine evolution process is characterized by a high current efficiency approaching 0.95 but a poor energy efficiency (about 0.3). As a consequence, a considerable quantity of heat must be eliminated and cooling coils are used to maintain a constant temperature of about 90 °C.

Although, the thermodynamic potential of HF decomposition is ca. 2.9 V [4,5], an anode–cathode voltage of about 8–10 V is necessary for obtaining the current density of 10–12 A dm^{-2} in industrial cells. For a cell working at 12 A dm^{-2}, the total voltage is composed of five contributions:

- reversible decomposition voltage (≈2.9 V);
- ohmic drop in the electrolyte (≈3 V);
- ohmic drop in the electrodes (≈0.5 V);
- cathode overvoltage (≈0.2 V);
- anode overvoltage (≈2.5 V).

The high anode overvoltage (≈2.5 V) is commonly ascribed to the formation of a solid carbon–fluorine layer on carbon anodes during fluorine production [1–8]. The inhibition of the fluorine evolution reaction (FER) is partly explained by the low surface energy of the film, which repels the electrolyte from the electrode. The contact angle is about 120–160° [9]: fluorine bubbles have a lenticular form and are strongly adherent to the carbon anodes surface. This induces a significant decrease in the electroactive surface area of the electrode. Qualitative evidence of the formation of a passivating layer on the carbon anodes is given by cyclic voltammetry studies [3,10,11] and X-ray photoelectron spectroscopy (XPS) [2,3,9,11–14]. Indeed, it has been previously established that the first voltammogram performed in KF–2HF with a new carbon anode exhibits an anodic passivation peak between 2.5 and 3.0 V versus Pt–H_2 which corresponds to the formation of a solid carbon–fluorine film (denoted C–F henceforth) at the anode surface. Many authors have concluded that the C–F film is composed of insulating graphite fluorides (denoted CF_x) and it was assumed that the electron transfer occurs by tunnel effect through the passive CF_x [15]: the latter acts as an inhibiting barrier for the electron transfer during the fluorine evolution reaction. It leads to very low values of transfer coefficient, in agreement with a mechanism involving electron tunneling through a passive film. For such a mechanism, the probability of electron transfer depends on the thickness and the height of the potential barrier. Many efforts were done to improve the fluorine evolution process. From these knowledge, the enhancement of the charge transfer rate may be performed by modifying the nature of the surface film. For instance, the modification of the local composition of the C–F film by inserting a metallic agent such as Al, Mg, ... gives rise to a beneficial effect [2,16–23]. The main goal of this treatment is to form locally fluorine–graphite intercalation compounds (denoted $C_{x'}F$ with $x' > 1$) which contain small traces of metal fluorides. The formation of such compounds reduces the influence of the CF_x groups on the global wettability of the electrode by KF–2HF and so, improves the fluorine bubbles detachment. However, one must notice that this beneficial effect is often limited for extended time. Childs and Bauer [24] have proposed a new design for the carbon anodes which contain vertical channels to enhance the movement of fluorine bubbles at the surface of the anode to the electrolyte surface. According to these authors, it is possible to operate at high current density for a very long time without polarizing. Moreover, the current efficiency was found to be near 100%.

Recently, the mechanism which occurs at the electrode/electrolyte interface was studied in detail; three main points have been reported [25–27].

1. The C–F film is mainly composed of conducting compounds belonging to the graphite intercalation compounds (GICs) family in which the C–F bonds are ionic and/or semi-ionic. Therefore, the fluorine evolution mechanism does not obey to a mechanism involving electron tunneling through a passive film as reported previously [15]: the electron can be easily transferred from the electrolyte to the electrode. Nevertheless, traces of insulating CF_x were also pointed out notably by scanning tunneling microscopy (STM) [25].
2. Mass transfer must be taken into account although the electrolysis of molten KF–2HF involves the main component of the melt (HF_2^-). Thus, the phenomena which govern the kinetics rate of the FER are: mass transfer and charge transfer [26].
3. As a consequence, a new model for the representation of the electrode/electrolyte interface has been proposed including the presence of an intermediate layer sandwiched between the C–F surface layer and the gaseous film [26,27]. This intermediate layer, called ''fluidized'' layer, is supposed to be composed of a mixed-phase comprising liquid KF–2HF and fluorine. Indeed, as in the case of hydrogen evolution in aqueous solution [28,29], one cannot exclude that this near-surface mixed-phase layer is supersaturated in fluorine gas.

These three points will be discussed in detail in the paper. At first, the electronic properties of the C–F film will be investigated using cyclic voltammetry, impedance measurements, X-ray photoelectron spectroscopy (XPS) and scanning tunneling microscopy (STM). Moreover, the influence of water in KF–2HF on the electronic properties and composition of the C–F film will be also discussed. Then, to understand how the current can flow at the electrode/KF–2HF interface even if a complete coating of the electrode by a fluorine gaseous film is observed, the influence of the mass transfer on the kinetics rate will be studied by chronoamperometry and impedance measurements using a rotating disk electrode. Finally, a new model for the representation of the electrode/electrolyte interface will be proposed. From

this model, the different contributions to the total anodic overvoltage will be determined using numerical calculations.

2. Results and discussion

2.1. Electronic properties of the C–F layer

Passive films formed on a metal surface may be semiconducting or insulating. Their electronic properties are generally described using the band model. The concentration of charge carriers is low in the case of a semiconductor and very low for an insulator. The value of the energy gap, E_g, defined as the difference between the bottom of the energy level of the conduction band and the top of the energy level of the valence band, is also used to distinguish an insulator and a semiconductor: for example, Ta_2O_5 which exhibits a large energy gap between 4.0 and 4.6 eV devoid of electronic states is considered as an insulator, and PtO, which has a gap of only 1.3 eV, is a semiconductor [30].

The electronic properties of the C–F film were investigated using impedance spectroscopy. However, for carbon anodes in molten KF–2HF, this aim is not easily reached: if the potential applied to the working electrode is greater than 2.9 V, fluorine evolution actually occurs and the impedance spectrum gives global information on the kinetics of the reaction in the presence of the solid carbon–fluorine film. Therefore, the experiments were not done under fluorine evolution in KF–2HF but in mercury. For these experiments, the fluorinated C–F film is located between two electronic conductors: carbon and mercury. Such structures belong to the M/O/M′-type structures, where M and M′ are two electronic conductors such as metals, and O a passivating film, usually the oxide of M. At first, the fluorination of the samples was done in KF–2HF and then the samples were tested in mercury.

The C–F films are usually considered as insulators. Therefore, if no potential is applied between C and C–F, the impedance measurement done with C/C–F/Hg structure should give rise to a capacitive behavior since only the dielectric properties of the C–F film is studied. But a surprising result was obtained: although, a 2–5 nm thick fluorinated surface layer was proved to be present by XPS measurements, and in spite of the supposed insulating properties of the C–F films, the Nyquist diagrams obtained in mercury with the C/C–F/Hg structures do not exhibit any capacitive loop. For instance, the spectrum obtained for non-graphitized (Le Carbone Lorraine) 205 NG passivated at 6 V in KF–2HF is presented in Fig. 1. It must be noted that this result does not depend on the variety of carbon materials (graphite, P2J industrial non-graphitized carbon ...) and the passivation mode of the carbon electrodes in well dehydrated ($C_{H_2O} < 20$ ppm) molten KF–2HF ($E = 2$, 3, 6 or 40 V). In each case, only an inductive and a resistive

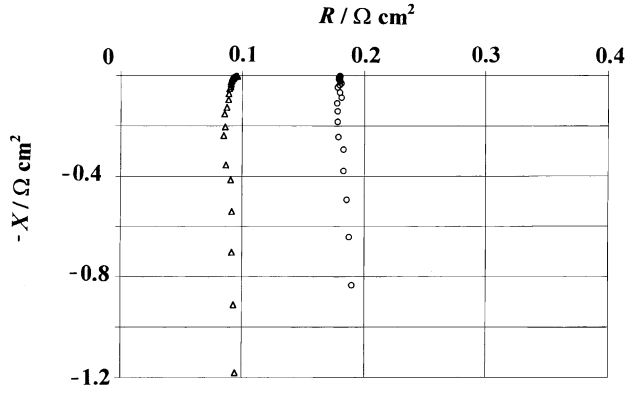

Fig. 1. Nyquist diagram obtained with a C/C–F/Hg structure ($S = 0.56$ cm^2); C–F layer was prepared in KF–2HF ($C_{H_2O} < 20$ ppm) at $E = 6$ V (denoted by △) or by chemical fluorination with F_2 gas in a furnace at 275 °C (denoted by ○). (Reprinted from [40].)

contribution due to the wires and to the ohmic resistance, respectively, were observed. Therefore, the C/C–F/Hg structure can be simply represented by an equivalent circuit composed of a high frequency resistance attributed to the ohmic resistance of the material and the surface film in series with an inductance. In the example presented in Fig. 1, the resistance is 0.096 Ω cm^2.

From these experiments, it was suggested that the solid C–F film formed on carbon anodes during electrolysis of molten KF–2HF exhibits electronic conductivity; therefore, it does not seem to constitute a high energy barrier for the electronic transfer for the fluorine evolution reaction: the electrons can be transferred easily through the surface film from Hg to the carbon substrate and vice versa. To confirm this assumption, cyclic voltammograms were obtained not in KF–2HF but in aqueous KCl solution in presence of the $Fe^{III/II}$ redox couple. First of all, and in order to valid the results obtained with C/C–F electrodes, the electron transfer rate of the $Fe^{III/II}$ redox couple was studied by cyclic voltammetry ($v = 20$ mV s^{-1}) using a platinum working electrode which was used as reference material (Fig. 2). Before recording voltammograms, several cycles were performed with the material in the range −1.1 to +0.7 V versus SCE to activate its surface [31]. Indeed, during this activation procedure, the thin oxide layer present at the surface of the metallic platinum electrode is progressively reduced. After this activation procedure, the potential difference, ΔE_p, between anodic and cathodic peaks was found to be about 65 mV. This value is very close to the theoretical one in the case of a reaction in which one electron is exchanged (60 mV). Rather similar ΔE_p values are obtained with non-porous vitreous carbon electrode previously passivated at 6 V in KF–2HF ($C_{H_2O} < 20$ ppm): $\Delta E_p \approx 70$ mV. It indicates that the electron transfer kinetics for the $Fe^{III/II}$ redox couple is rapid and confirms our previous results deduced from impedance measurements in mercury: the C–F film behaves like an electronic conductor and cannot be considered as insulating for the electron transfer.

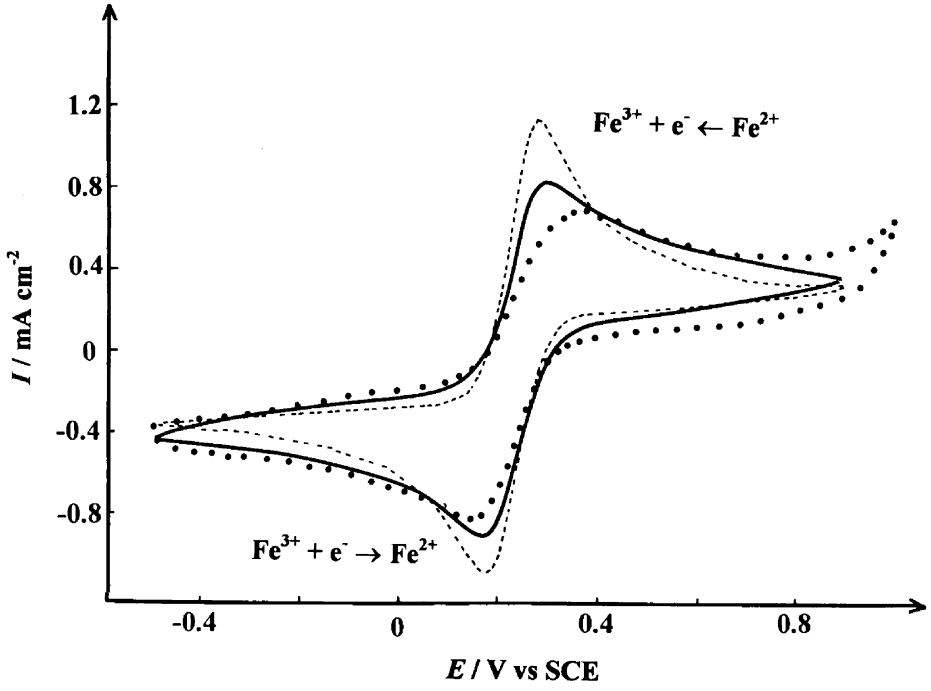

Fig. 2. Cyclic voltammograms ($v = 20$ mV s^{-1}) obtained in 1 M KCl + 10^{-2} M $K_3Fe(CN)_6/K_4Fe(CN)_6$. (- - -): Pt electrode; (—): carbon passivated at 6 V in KF–2HF ($C_{H_2O} < 20$ ppm); (●●●●●): carbon chemically fluorinated with F_2 gas in a furnace at 275 °C. (Reprinted from [40].)

2.2. Nature of the C–F layer

STM experiments were performed to study the local conductivity of the surface C–F film. These experiments were performed using HOPG in order to reach the nanometric scale. Typical hexagonal symmetry was observed with pure HOPG (Fig. 3a) after cleavage [32]. Only half of the carbon atoms of a graphene layer exhibit high electronic density, due to the non-equivalence of the atomic sites resulting from the ABAB stacking of graphene layers. In the case of HOPG electrochemically fluorinated in KF–2HF at 6 V, the approach of the tip cannot be done in many parts of the surface since no current was detected, even for high bias values. These parts of the electrode surface were called domains "A" and are composed of very insulating CF_x.

In most part of the conducting electrode surface, two kinds of images are clearly distinguished indicating the formation of GICs. In the domains "B", all the carbon atoms of the hexagonal rings are observed. The spacing between two neighboring atoms deduced from the corrugation amplitudes given in Fig. 3b is about 0.154 nm. For explaining such a modification compared to pure HOPG, one can suppose that the intercalation of HF_2^- species increases the distance between two carbon sheets. Moreover, the plan situated just below the surface is occupied by HF_2^- intercalants. In the domains "C", the same hexagonal symmetry as that of HOPG was observed, with a periodicity of 0.244 nm (Fig. 3c). A schematic representation of the hexagonal lattice commensurate with the graphite lattice is shown in Fig. 4. By contrast with pure HOPG, an overlap of the electronic densities between two neighboring atoms was observed (Fig. 3b and c). The literature mentions some results obtained by STM with fluorinated HOPG prepared by chemical reaction of F_2/HF mixture with HOPG at room temperature [33]. In that case, a new non-centered hexagonal symmetry was formed. However, in spite of carbon atoms are bonded to intercalated fluorine atoms, each atom is well separated from the others in terms of electronic density as for pure HOPG. In our case, one may suppose that the fluorination of the surface coupled with the intercalation of HF_2^- anion between two carbon sheets induce the formation of C–F bonds which modify the electronic densities of each carbon atom. The overlap of the electronic densities observed in Fig. 3c results of two neighboring F atoms as proposed in the schematic representation of the in-plane structural model of fluorinated HOPG illustrated in Fig. 4.

The C–F film is an electronic conductor and mainly composed of conducting compounds belonging to the graphite intercalation compounds (GICs) family in which the C–F bonds are ionic and/or semi-ionic. The wettability of these compounds by KF–2HF is usually high; nevertheless, the C–F film formed in KF–2HF does not have such a property. The C–F film contains a small amount of CF_x. In order to study the exact influence of the CF_x groups present in the C–F layer on the FER, results obtained with carbon anodes electrochemically passivated in KF–2HF and chemically passivated in a furnace at 275 °C under pure fluorine atmosphere ($p_{F_2} = 1$ atm) were compared. Indeed, it is well known that fluorine strongly reacts with carbon at a moderate temperature to form CF_x. *I–E* curves obtained with

these samples are presented in Fig. 5. Significant differences between these two preparation modes were observed: in the case of crude carbon, the fluorine evolution reaction takes place even if a high anodic overvoltage was observed. In the case of a carbon electrode fluorinated with elemental fluorine, the fluorine evolution reaction in KF–2HF is completely inhibited even at high potentials. The chemical fluorination of carbon anode using fluorine gas seems to give rise to the formation of a more resistive surface layer. However, impedance measurements in mercury performed

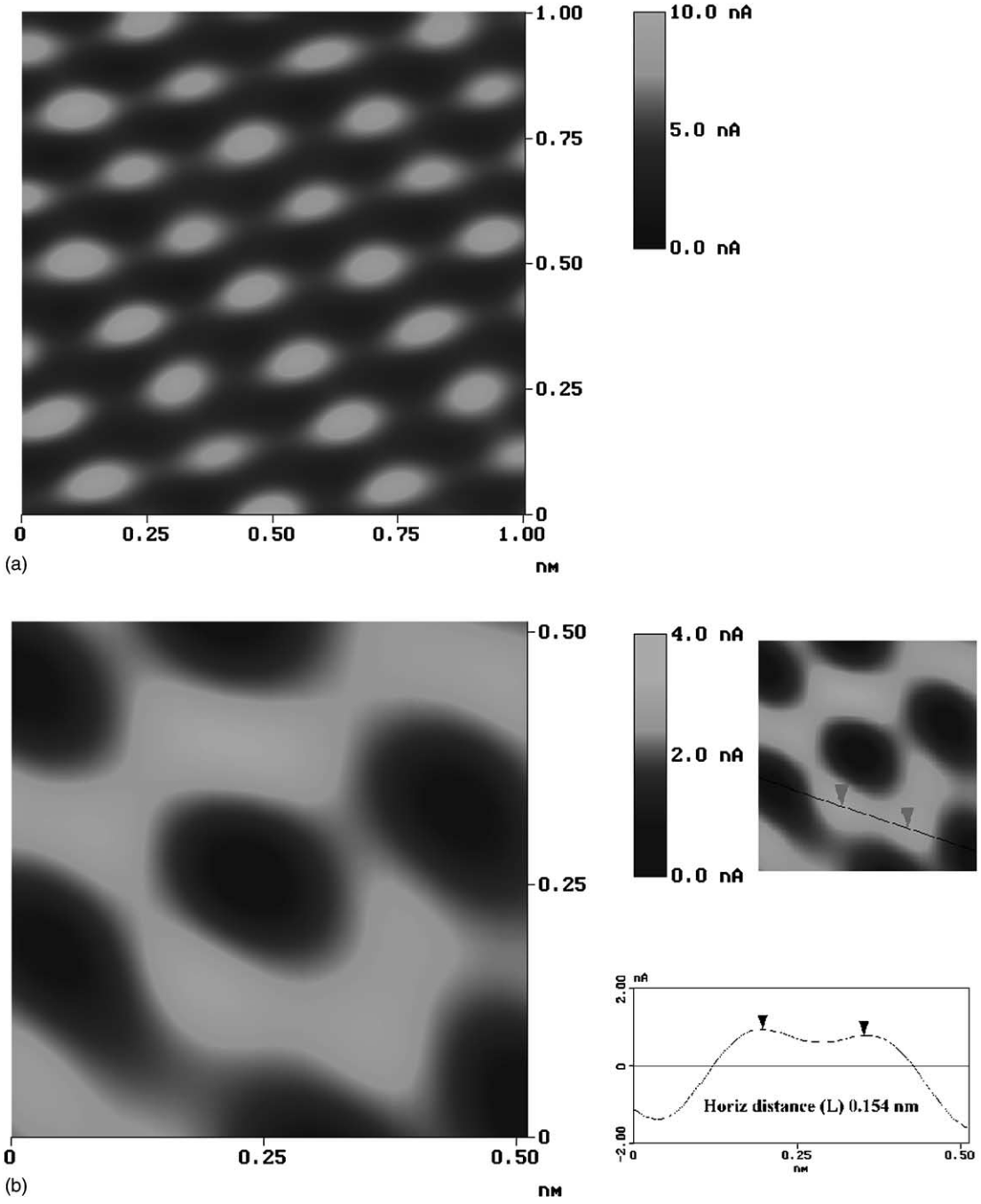

Fig. 3. (a) STM image of pure HOPG. Experimental conditions: bias voltage: 20 mV; setpoint: 4 nA; z range: 5 nA; constant-height mode; Pt/Ir tip. (b) STM image and cross section of HOPG passivated at 6 V in KF–2HF ($C_{H_2O} < 20$ ppm) during 30 min; domain "B" showing all the carbon atoms of the layer in the hexagonal ring. Experimental conditions: bias voltage: 20 mV; setpoint: 4 nA; z range: 5 nA; constant-height mode; Pt/Ir tip. (c) STM image and cross section for HOPG passivated at 6 V in KF–2HF ($C_{H_2O} < 20$ ppm) during 30 min; domain "C" showing half of the carbon atoms of the layer with overlap of electronic densities. Experimental conditions: bias voltage: 20 mV; setpoint: 4 nA; z range: 3 nA; constant-height mode; Pt/Ir tip. (d) STM image of HOPG passivated at 6 V in KF–2HF ($C_{H_2O} \approx 600$ ppm) during 30 min. Experimental conditions: bias voltage: 15 mV; setpoint: 5 nA; z range: 5 nA. (e) STM image of HOPG fluorinated by F_2 gas at 275 °C. Experimental conditions: bias voltage: 20 mV; setpoint: 5 nA; z range: 5 nA. (Images in sections a, d and e are reprinted from [40]. Images in section (b) and (c) are reprinted from [25].)

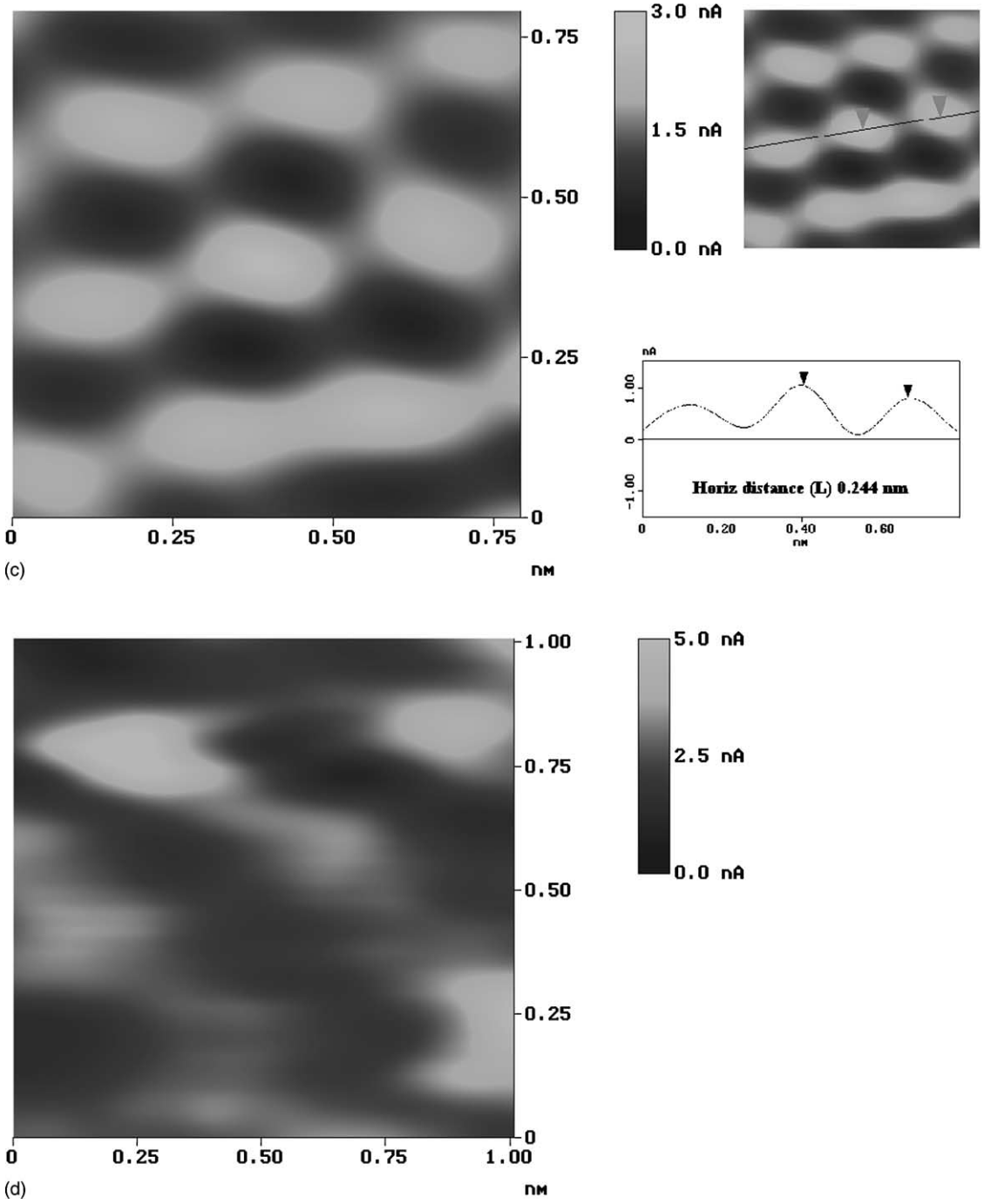

Fig. 3.. (*Continued*).

with carbon electrode chemically fluorinated with pure fluorine have shown that the Nyquist diagrams (Fig. 1) do not exhibit any capacitive loop. In spite of the presence of the fluorinated surface layer which blocked the electron transfer during the FER, only an inductive contribution attributed to the wires, and a resistive contribution attributed to the ohmic resistance of the material and the surface film are observed. The resistance is equal to 0.184 Ω cm^2. This value is about two times higher than that obtained in the case of carbon samples fluorinated in KF–2HF. Nevertheless, the shape of the Nyquist diagrams indicates that the electrons can be transferred from Hg to the carbon substrate and vice versa, i.e. the surface film exhibits electronic conductivity.

XPS measurements performed with samples fluorinated in KF–2HF and with F_2 as described above allows to understand such different behavior from the analysis of high resolution spectra of the F1s region. The individual fitting parameters (BE and FWHM) as well as the relative contribution of each group (I_i/%) to the total area under the peak for the F1s region are presented in the case of the chemical

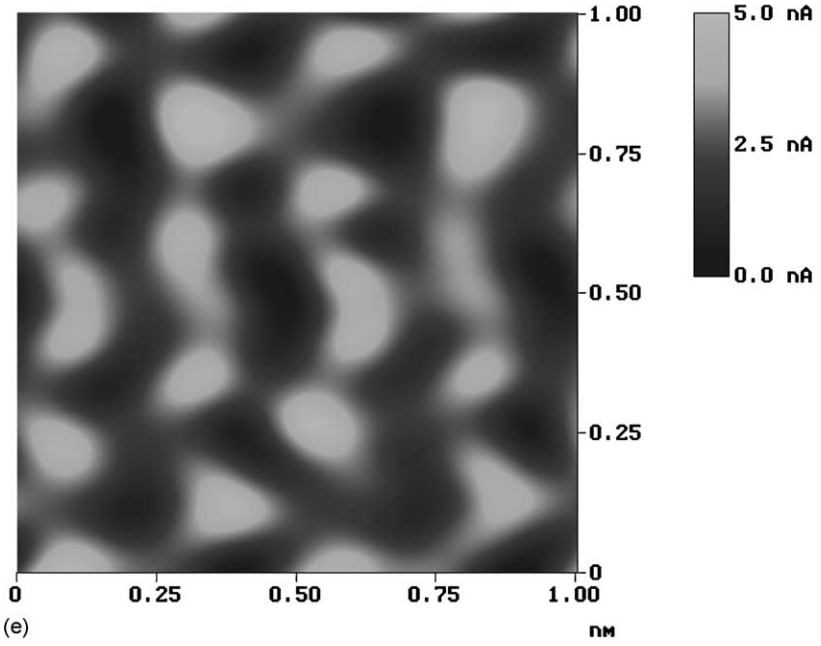

Fig. 3.. (*Continued*).

and the electrochemical fluorinated samples in Table 1. The detailed analysis of the high resolution spectra of F1s region are presented in Fig. 6a and b. For sample passivated in KF–2HF, the peak located at 688.6 eV corresponds to semi-ionic C–F bonds: the reversible electrochemical intercalation of HF2-species into the carbon lattice occurs at low potential [9] (≤3 V), forming $C_{x'}(HF)_yF$(FIC) according to:

$$x'C + HF_2^- + (y-1)HF \Leftrightarrow C_{x'}(HF)_yF + e^- \quad (5)$$

If $y = 1$, the compound reported in Reaction (5) is sometimes denoted $C_{x'}{}^+HF_2^-$. This formula shows that the positive charge is delocalized on x' carbon atoms. Similar compounds have been already synthesized by the chemical reaction of fluorine gas with carbon in presence of a suitable catalyst as HF. In such compounds, the anions are mobile and the carbon–fluorine bonds are ionic or semi-ionic [9]. The electrochemical behavior of carbon anodes subjected to fluorine production probably strongly depends on the intercalation step (Reaction (5)). Indeed, during cyclic voltammetry experiments performed in a low potential range (0–3 V), the electrochemical intercalation of fluoride ions into the carbon lattice and the fluorination of carbon atoms bonded to hydrogen, oxygen, OH, or to >C=O leaving groups occur together [7,34,35]. Thus, the anodic peak in cyclic voltammetry is attributed both to the intercalation phenomenon and to the formation of a carbon–fluorine passivating layer. During the reverse scan, a reduction peak is observed. It corresponds to the reduction of $C_{x'}(HF)_yF$ (partial deintercalation of HF_2^- ions). This intercalation–deintercalation reaction is clearly visible with graphite for which the anodic peak can be 100 times larger than that obtained with amorphous carbon; the lamellar structure of graphite allows the deep penetration of HF_2^- ions into the bulk of the electrode. This insertion may be responsible for the swelling of graphite electrodes in KF–2HF melt. A decrease of the stage number of $C_{x'}(HF)_yF$ and a decrease of the x' values are observed with an increase of the applied potential. So, the reduction of the compound formed at high potential is more and more difficult.

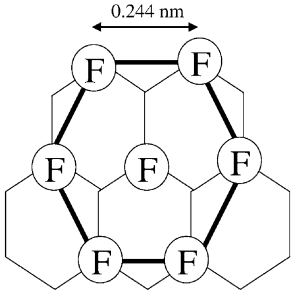

Fig. 4. Schematic in-plane structural model for fluorinated HOPG. The centered hexagonal lattice commensurate with the graphite lattice is shown. Open circles: bonded C atoms. (Reprinted from [25].)

For the sample chemically fluorinated at 275 °C, the main peak of the F1s region (Fig. 6b) is shifted towards higher values of binding energies. The peaks observed at 689.3 eV corresponds to semi-ionic C–F bonds. For that sample, another peak is observed at 692.8 eV due to covalent C–F bonds in CF_x. The formation of covalent carbon–fluorine bonds results from the fluorination of carbon atoms bonded to hydrogen, oxygen, OH, . . . Finally, note that in the case of chemical fluorination, a strong distortion of the hexagonal structure of the starting material was also pointed out (Fig. 3d). It is well known that during the formation of

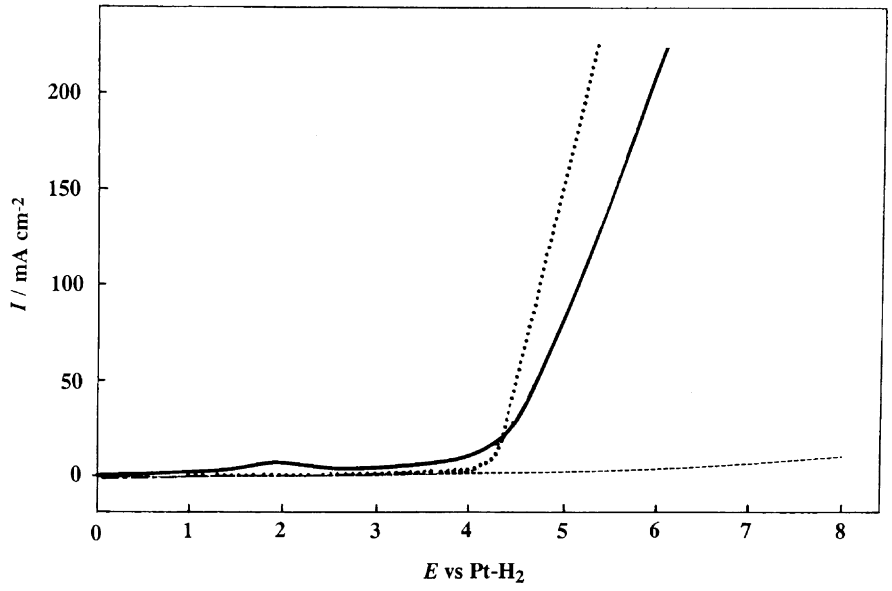

Fig. 5. *I–E* curves ($v = 0.4$ V s^{-1}) obtained in KF–2HF ($C_{H_2O} < 20$ ppm). (—): carbon after electrochemical passivation in KF–2HF; (· · ·): carbon after electrochemical activation in KF–2HF at 40 V during 1 min; (- - -): carbon fluorinated with fluorine gas at 275 °C ($S = 5.5$ cm^2).

graphite fluorides at $T > 350$ °C, the chair-structure of cyclohexane in which the chemical bond was completely changed to sp^3 is observed. In our case, the temperature of the reaction ($T = 275$ °C) is lower and therefore, the images presented in Fig. 3d should correspond to an intermediate step between the hexagonal symmetry of pure HOPG and the structure of graphite fluorides.

The results presented in this paragraph have confirmed our assumptions about the heterogeneities of composition of the C–F surface film formed in well dehydrated molten KF–2HF: the C–F film is mainly composed of conducting GICs, in which carbon atoms are bonded to fluorine atoms and induced an overlap of the electronic densities as revealed by STM measurements; these experiments have also pointed out the presence of insulating CF_x in some parts of the surface. Nevertheless, the amount of CF_x is expected to be very low at the surface of carbon anode passivated in KF–2HF since the F1s region does not exhibit any covalent C–F bond, as in the case of a chemical fluorination. But, even if the CF_x amount is very low, it is enough to limit drastically the wettability by KF–2HF and to explain the high adherence of the fluorine bubbles on the surface.

2.3. Influence of water in KF–2HF on the electronic properties of the C–F layer

As mentioned above, water contained in KF–2HF is reported to have a significant influence on the fluorine evolution reaction since water promotes anode effect [34,36]. Water in KF–2HF contributes to the electrogeneration of graphite oxide according to:

$$zC + (1+y)H_2O \rightarrow C_zO(OH)_y + (y+2)H^+ + (y+2)e^- \quad (6)$$

Graphite oxides are easily fluorinated at room temperature because of their high instability. Thus, for increasing potentials applied to the carbon electrodes in KF–2HF, oxygen in $C_zO(OH)_y$ groups might be easily exchanged with fluorine and give rise to large amounts of insulating graphite fluoride [34,36] according to:

$$C_zO(OH)_y + (2+xz+3y)F^- \rightarrow zCF_x + (1+y)F_2O + yHF + (2+xz+3y)e^- \quad (7)$$

Table 1
Results of XPS investigations for carbon electrochemically passivated at 6 V in KF–2HF ($C_{H_2O} < 20$ ppm) and carbons chemically fluorinated with F_2 gas at 275 °C

Chemical states	Carbon fluorinated in KF–2HF ($C_{H_2O} < 20$ ppm)			Carbon fluorinated by F_2 gas		
	BE (eV)	FWHM (eV)	I_i (%)	BE (eV)	FWHM (eV)	I_i (%)
Semi-ionic C–F	688.6	2.6	100	689.3	2.3	74
Covalent C–F	–	–	–	692.8	3.3	26

Fitting parameters of the F1s region. Binding energy values (BE/eV) without correction of charge effect, full width at half-maximum (FWHM/eV), relative contribution of each group in the same sample (I_i/%).

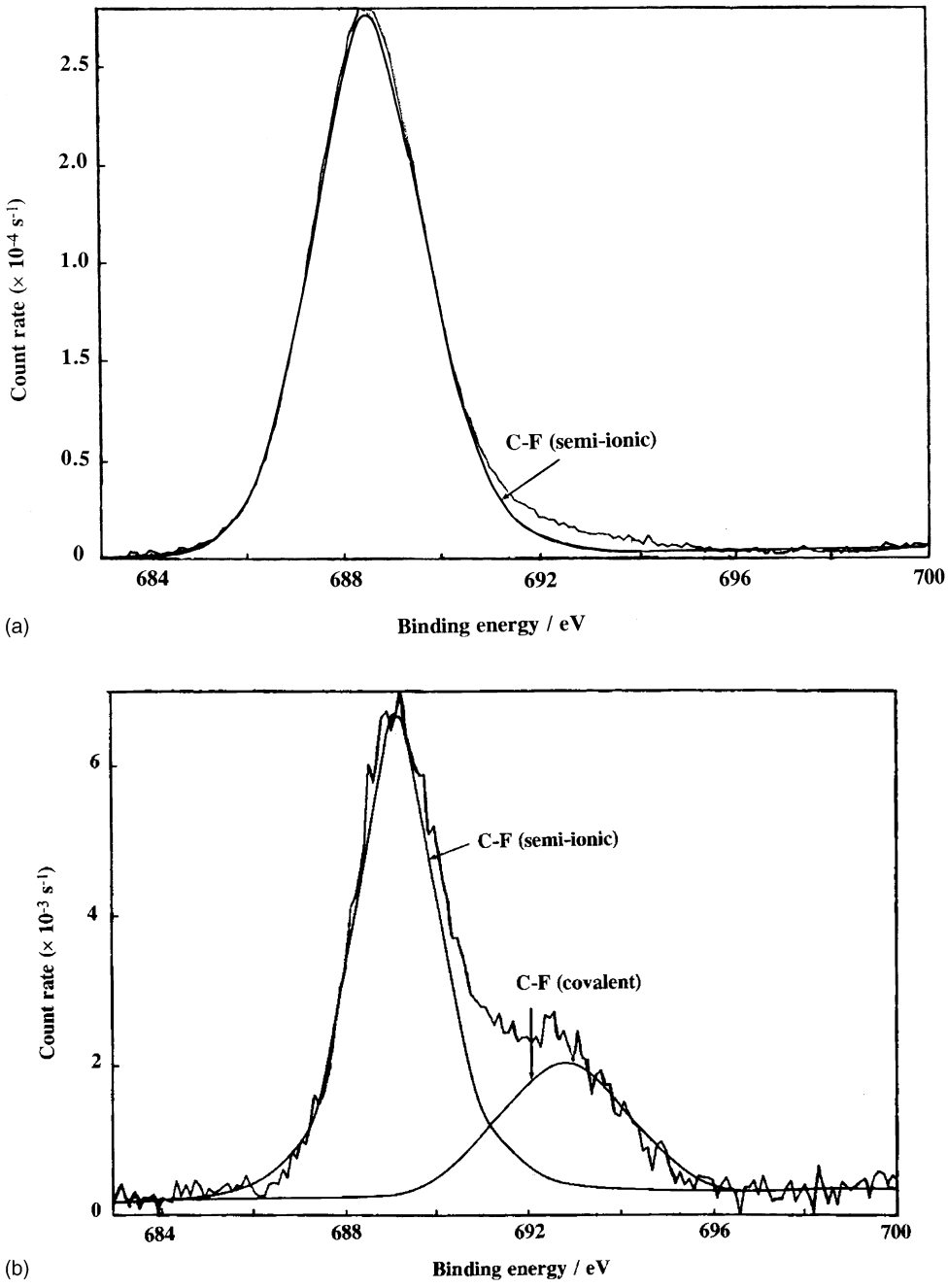

Fig. 6. XPS analysis. High resolution spectra of the F1s region. (a) Carbon after electrochemical passivation in KF–2HF ($C_{H_2O} < 20$ ppm); (b) carbon fluorinated with fluorine gas at 275 °C. (Reprinted from [35]. Reproduced by permission of The Electrochemical Society Inc.)

If the water concentration into KF–2HF increases, the amount of CF_x on the surface of carbon electrodes should increase. Consequently, the electronic properties of carbon electrodes passivated in a KF–2HF melt containing a higher water concentration should be strongly modified.

In order to confirm this assumption, the electronic properties of the C–F film formed on non-porous vitreous carbon electrode passivated in molten KF–2HF with a water concentration of about 600 ppm were studied; these results were compared with those obtained with carbon passivated in a well dehydrated molten KF–2HF for which $C_{H_2O} < 20$ ppm, and with fluorine gas at 275 °C as described above. Then, the passivated electrode was tested by cyclic voltammetry in 1 M KCl containing 10^{-2} M $K_3Fe(CN)_6/K_4Fe(CN)_6$ to study the kinetics of the $Fe^{III/II}$ reaction. As shown in Fig. 2, the potential difference value, ΔE_p, between the anodic and the cathodic peaks is close to 180 mV. This value is about 2.6 times higher than that obtained in the case of carbon electrodes previously passivated in well dehydrated molten KF–2HF ($\Delta E_p \approx 70$ mV) but close to that

obtained with sample chemically fluorinated at 275 °C ($\Delta E_p \approx 205$ mV).

Finally, STM measurements performed with sample passivated in KF–2HF containing about 600 ppm of water gives rise to the following observations: (i) the approach of the tip cannot be done since no current was detected, even for high bias values due to the presence of insulating graphite fluorides; (ii) conducting areas are also detected but the hexagonal structure of HOPG is completely lost as illustrated in Fig. 3e.

2.4. Influence of the mass transfer on the kinetics rate of the FER

The mechanism of bubbles evolution involves usually the formation of a gas-supersaturated solution (with H_2 for example) in the region near the electrode/electrolyte interface, from which the gas diffuses away [37]. In that region, the formation of small bubble nuclei occurs at nucleation sites which correspond generally to imperfections of the surface. The gas formed at the electrode is dissolved in the electrolyte which becomes supersaturated. Then, the bubbles grow to a certain size and then move away. In situ observations were performed in KF–2HF with an electrochemical cell equipped with a Plexiglas window, which made visible inspection possible as shown in Fig. 7. In this figure, only the upper part of the surface is electroactive and the other part of the electrode is covered by insulating Teflon. Almost all the electrode surface is covered by bubbles (Fig. 7) [9,27,38]; nevertheless, high value of current can flow at the electrode/electrolyte interface. To explain such phenomenon, the influence of mass transfer on the kinetics of the FER was studied by impedance spectroscopy and amperometry. These experiments were performed in KF–2HF using a rotating disk electrode facing the bottom of the electrochemical cell.

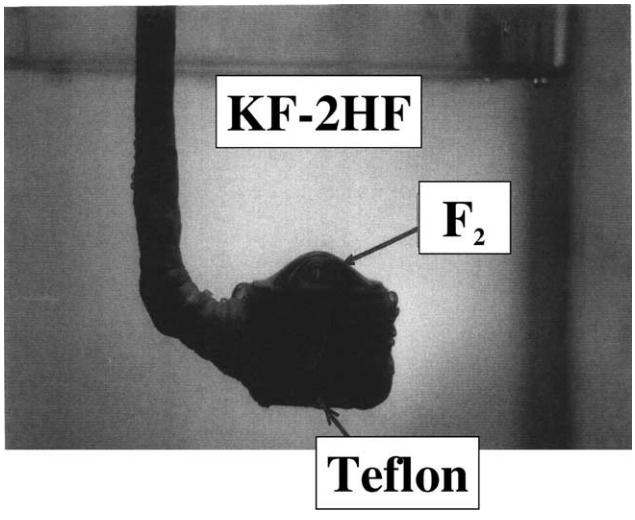

Fig. 7. Evolution of fluorine in KF–2HF ($C_{H_2O} < 20$ ppm) on a horizontal carbon electrode ($S = 2$ cm^2) facing the top of the electrochemical cell ($E = 5$ V vs. Cu/CuF_2). (Reprinted from [26]. Reproduced by permission of The Electrochemical Society Inc.)

A typical impedance spectrum obtained at 3.7 V versus Cu/CuF_2 for $\omega = 3000$ rpm is presented in Fig. 8a. Two distinct capacitive loops are observed at high frequencies and low frequencies. The high frequency resistance, denoted R_{HF}, is given by the diameter of the first semi-circle. The variation of $R_{HF} = f(E)$ in the whole ω range is presented in Fig. 8b. Usually, in the case of a system controlled by charge transfer, the associated charge transfer resistance, R_f, tends to 0 for high overvoltages; in the present case, even for high E and whatever the ω value, R_{HF} tends to a finite value $R_0 = 3.9\ \Omega$. The impedance diagrams in the Bode representation ($|Z_{Im}| = g(f)$ with $f = \omega/2\pi$) given in Fig. 8c for $\omega = 1000$ rpm show the existence of a shoulder at around 200 kHz in all the E range. This contribution becomes predominant with increasing E values and appears to be the only one at highest E values. To interpret these results, one have concluded that the first loop at high frequency is in fact composed of two overlapped semi-circles: the first one at very high frequency has a characteristic frequency of about 200 kHz and a constant diameter equal to $R_0 = 3.9\ \Omega$. The second one, observed in the middle frequency range, is related to the charge transfer associated to the FER. The charge transfer resistance, R_f, given by the diameter of the semi-circle for low potential value decreases exponentially with E for reaching a null value for high E. In the present case, the fitting is a necessary step to determine all the electric components because of the overlap of these two semi-circles. The fitting of the experimental curve for the high frequency part was done considering an electric equivalent circuit composed of R_s, electrolyte resistance, in series with two loops (R_0, C_0) and (R_f, C_f). C_f is related to the C–F film.

Another semi-circle was observed at low frequency due to mass transfer (Fig. 8a). This semi-circle is characterized by a low frequency resistance, R_{LF}, which corresponds to the diameter of the semi-circle. The variations of $R_{LF} = (E, \omega)$ presented in Fig. 8d show a decrease of R_{LF} with increasing ω values, i.e. the mass transfer of electroactive species to the surface is accelerated.

From these experiments, it seems very clear that the kinetics of the fluorine evolution reaction is not only controlled by charge transfer but also by mass transfer.

2.5. Representation of the electrode/electrolyte interface

The parameters R_0 and C_0 defined above cannot be attributed to the resistance and the capacitance, respectively of the fluorine gas film present on the surface since the high electric resistivity and the thickness of elemental F_2 gaseous film should give rise to a higher resistance value than $R_0 = 3.9\ \Omega$. Therefore, for a better understanding of the obtained results, we have proposed a new model for the description of the electrode/electrolyte interface (Fig. 9) in which a thin layer, composed of a mixture of KF–2HF and

F_2, is sandwiched between the electrode surface and the gaseous film. This layer, which is called "fluidized" layer henceforth, is characterized by R_0 and C_0; it presents an electrical resistivity higher than the single phase KF–2HF but lower than elemental fluorine, and should give rise to an additional resistive contribution which increases the anodic overvoltage. In this model, the electroactive species (HF_2^-) as well as K^+ and HF present in the electrolyte diffuse simultaneously under the gaseous film via the lateral sides of the electrode. Thus, the electroactive species are consumed in the intermediate layer. The rising of bubbles causes also a circulation of electrolyte. This assumption explains the shape of the *I–E* curve recorded with a rotating disk electrode in KF–2HF; for instance, the variation $I = f(E)$ for $\omega = 5000$ rpm and for a linear variation of the potential versus time ($v = 1$ mV s^{-1}) is presented in Fig. 10: a S-shaped curve is observed as when a rotating disk electrode is used for studying a system for which the mass transfer is controlled by diffusion. Nevertheless, in our case, the I plateau is not clearly defined because of the too high quantity of fluorine bubble present at the surface for $E > 4.9$ V: the electroactive surface area is completely blocked.

2.6. Mechanism of the fluorine evolution process

The fluorine evolution reaction was also studied by chronoamperometry on a horizontal carbon anode facing

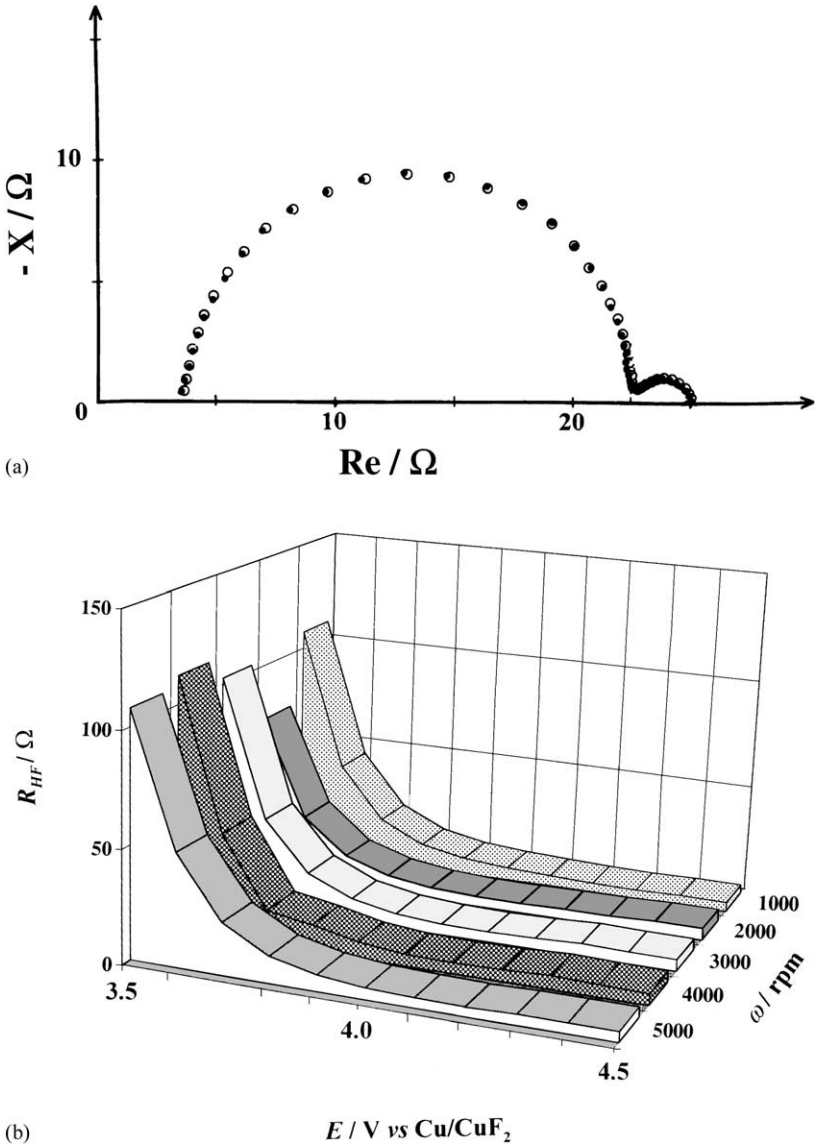

Fig. 8. Results deduced from impedance measurements performed in KF–2HF ($C_{H_2O} < 20$ ppm) with a rotating disk electrode ($S = 0.79$ cm^2). (a) Nyquist diagram: $\omega = 3000$ rpm; $E = 3.7$ V vs. Cu/CuF_2; (●): experimental data; (○): simulated data. (b) Variation of the high frequency resistance, R_{HF}, vs. E (in all the ω range). (c) Evolution of the impedance diagrams in Bode representation ($\omega = 1000$ rpm). (d) Variation of the low frequency resistance, R_{LF}, vs. E (in all the ω range). All the data presented in (b) and (d) were deduced from the fitting of impedance spectra. (Reprinted from [26]. Reproduced by permission of The Electrochemical Society Inc.)

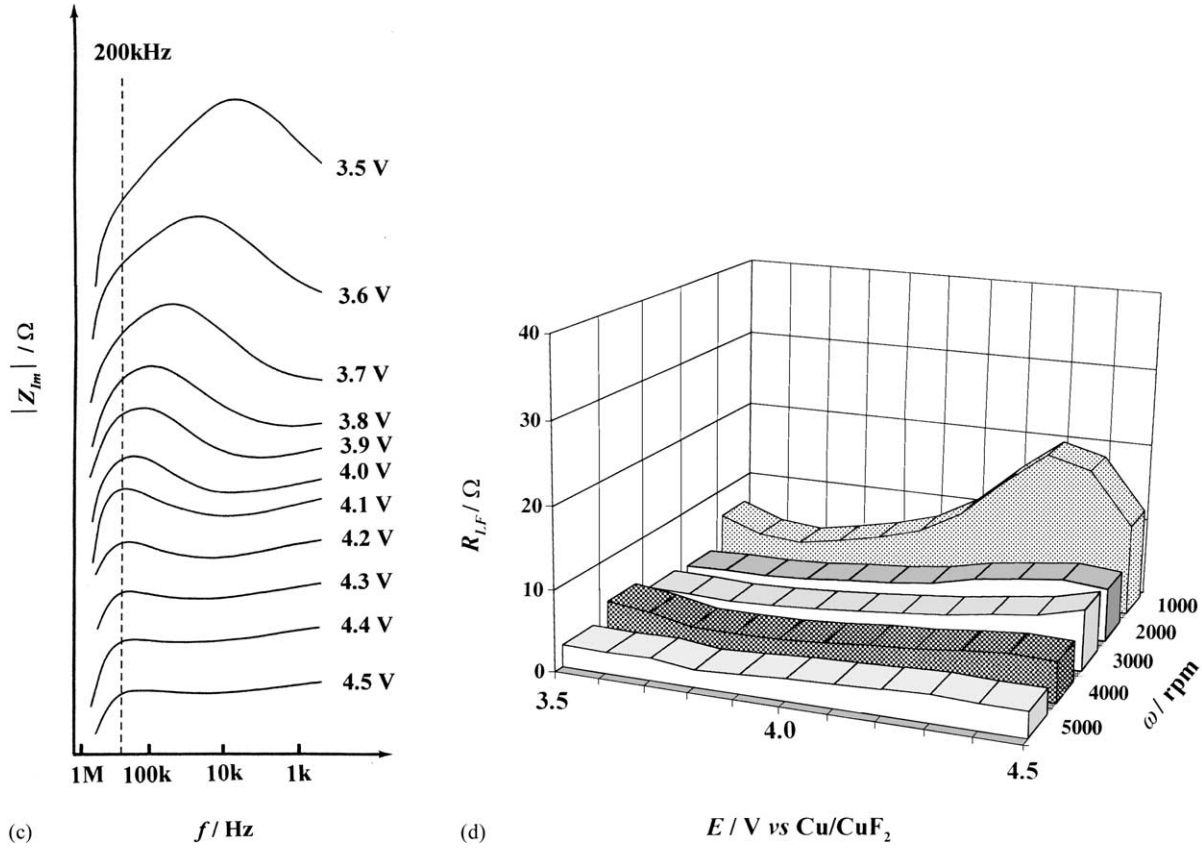

Fig. 8.. (*Continued*).

the top of the electrochemical cell as described in Fig. 7. A typical $I = f(t)$ curve obtained in KF–2HF at $E = 4.5$ V is presented in Fig. 11. A schematic evolution of fluorine in KF–2HF with such electrode is illustrated in Fig. 12. At $t = 0$, a potentiostatic step is applied to the electrode (Fig. 12a); the current density reaches rapidly a maximum value. Small fluorine bubbles are formed on imperfections on the electrode surface and into the pores of the electrode. When one pore is filled with fluorine, the gas spreads on the flat part all around the pore; the phenomenon occurs in the nearest pores and recombination of the gaseous bubbles is observed (Fig. 12b). It results in a decrease of the electroactive area and correlated decrease of the current density. Then, coalescence of the gaseous bubbles occurs. Concomitant to that recombination, the formation of the ''fluidized'' layer under each bubble occurs. The current density decreases until reaching a constant value different from zero which corresponds to the total coverage of the electrode (Fig. 12c). Then, the bubble elongates (Fig. 12d) according to the mechanism described above which considers the diffusion of the electroactive species in the ''fluidized'' layer sandwiched between the upper fluorine gas and the carbon surface. The electroactive species (HF_2^-), K^+ and HF diffuse under the gaseous film via the lateral sides of the electrode. This model explains why the current density never reaches a null value: electroactive species are always present near the carbon surface in the ''fluidized'' layer. In addition, after detachment, the current density never reaches the maximum current density value observed at the beginning of the chronoamperogram since fluorine gas is always present on the carbon surface, notably inside the pores; the electroactive surface is then lower than that at the beginning of the first potential step. When the volume of the fluorine bubble reaches its maximum value (Fig. 12e), the gas bubble escapes from the surface (Fig. 12f) and the current density jumps to a maximum value, lower than the first one. Then the phenomenon becomes perfectly cyclic: the fluorine bubble evolution restarts (Fig. 12c) from the same nuclei, and so on; the surface shining suggests that the ''fluidized'' layer remains on the electrode after the bubble departure.

It is probable that the electrochemical reaction does not take place at the whole surface but at a ring situated at the edge of the electrode. In order to verify this assumption, complementary experiment was performed using a ring-disk electrode: the center and the external surfaces of the electrode were separated by a very thin insulating Teflon ring. Both parts of the electrode could be polarized independently or simultaneously. The current density (Fig. 13) at the center of the electrode is recorded versus time. At first, only the center of the electrode is polarized at a constant potential of 6 V (Fig. 13). After 10 min, a constant current of

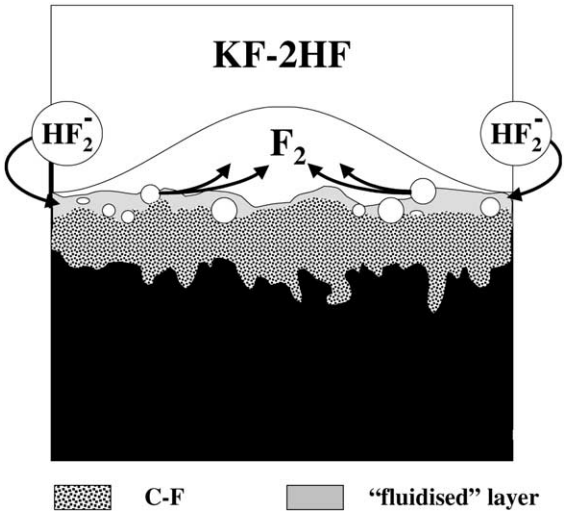

Fig. 9. Schematic representation of the carbon/KF–2HF interface. Cross section of an horizontal carbon electrode facing the top of the electrochemical cell. A ''fluidized'' layer in which co-exist liquid KF–2HF and fluorine gas is sandwiched between the C–F film and F_2 bubble. A gradient of concentration of fluorine in the solid C–F layer up to the surface of the carbon electrode is observed. (Reprinted from [26]. Reproduced by permission of The Electrochemical Society Inc.)

$I_{ext} = 500$ mA is simultaneously applied to the external surface; the current density at the center of the electrode decreases drastically although 6 V potential is still applied to the center of the electrode. It clearly demonstrates that the electroactive surface area involved in the fluorine evolution reaction is constituted of a ring at the edge of the electrode; the center is rather completely inactive.

2.7. Determination of the different contributions to the anodic overvoltage

The results presented above have revealed the significant influence of the ''fluidized'' layer in the fluorine evolution process. Thus, it seems to be obvious that the high anodic

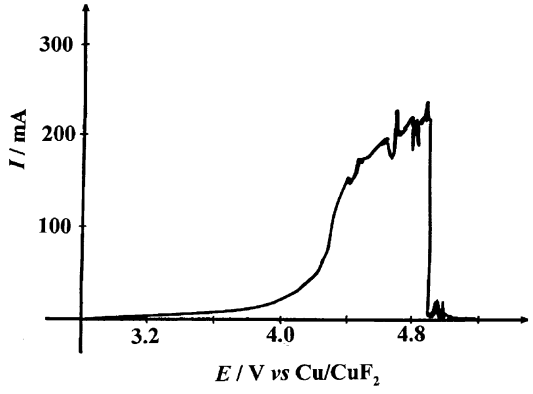

Fig. 10. Quasi-stationary I–E curves ($v = 1$ mV s^{-1}) obtained in KF–2HF ($C_{H_2O} < 20$ ppm) with a rotating disk electrode ($\omega = 5000$ rpm; $S = 0.79$ cm^2). (Reprinted from [26]. Reproduced by permission of The Electrochemical Society Inc.)

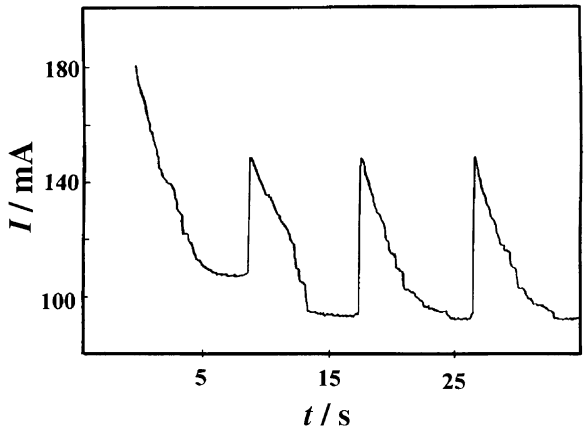

Fig. 11. Variation of I vs. t obtained in KF–2HF ($C_{H_2O} < 20$ ppm) with an horizontal carbon electrode ($S = 2$ cm^2) facing the top of the electrochemical cell ($E = 5$ V vs. Cu/CuF_2). (Reprinted from [26]. Reproduced by permission of The Electrochemical Society Inc.)

overvoltage, η_T, which characterizes the FER is not only due to the C–F film present on carbon anodes but also to the ''fluidized'' layer. Therefore, η_T is composed of η_{C-F} (activation overvoltage for the fluorine evolution reaction) and η_{fluid} (ohmic drop in the ''fluidized'' layer):

$$\eta_T = \eta_{C-F} + \eta_{fluid} \quad (8)$$

These results must be related to those reported in the literature [39] on laser Doppler velocimetry measurements performed in KF–2HF at the immediate vicinity of the electrode during fluorine evolution. These experiments have shown that: (i) the electrode appeared always covered by a very thin uniform colorless film that was at first supposed to be pure fluorine gas; (ii) its thickness, δ, carefully measured by optical means for several current densities, was found to be constant ($\delta \approx 0.03$ cm); (iii) the electrolyte acceleration along the electrode was found constant like for the gaseous phase. The author has concluded that, at the vicinity of the electrode, the gaseous film interacts very strongly with the dense electrolyte and lifts it at the same velocity. These conclusions are in a very good agreement with our results except for the composition of the media in which fluorine bubbles are evacuated: the region near the electrode surface in the electrolyte is supposed to be composed of a mixture of KF–2HF and dissolved fluorine instead of pure fluorine gas. However, the thickness δ which was measured is not the thickness of the gaseous surface film but the thickness of the ''fluidized'' layer.

To obtain a quantitative description of the phenomenon, a model is developed and the reaction mechanism is analyzed by numerical simulation. Its aim is to determine the exact contribution of η_{fluid} and η_{C-F} to η_T. To succeed, we have considered a schematic representation of the electrode/electrolyte interface in which the current flows through a conductive disk (''fluidized'' layer) by the lateral sides. This disk covered by a fluorine bubble has a constant radius, r_0, a constant thickness, δ, and a resistivity, ρ. The disk is divided

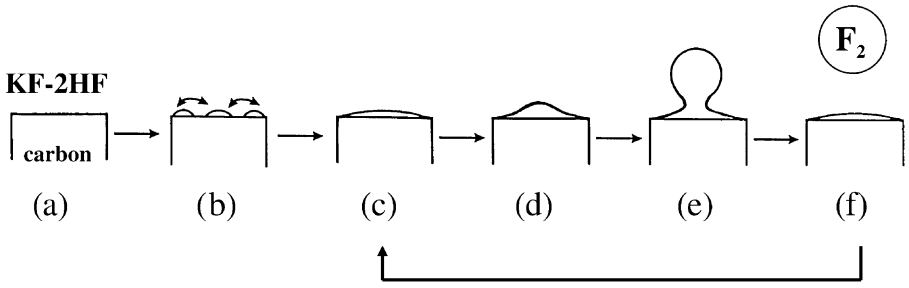

Fig. 12. Schematic evolution of fluorine in KF–2HF on horizontal carbon electrode facing the top of the electrochemical cell. (Reprinted from [26]. Reproduced by permission of The Electrochemical Society Inc.)

into 1000 elemental rings of thickness $dr = r_0/1000$. The current–potential relationship follows the Butler–Volmer's law in which the contribution of the reduction part is neglected since high anodic overvoltages is considered. The contribution to the current of each elemental ring of thickness dr is:

$$dI = 2\pi r j\, dr \tag{9}$$

where j is the current density.

The integration of Eq. (9) between 0 and r_0 gives the total current, I_T. η_{fluid}, is considered to be an ohmic-type overvoltage which takes into account the resistivity, ρ, of this layer. Then, for each elemental ring of thickness dr, one has:

$$d\eta_{fluid} = \rho \frac{I}{2\pi r \delta} dr \tag{10}$$

The total overvoltage defined in relation (8) is constant and fixed at 2.5 V; the thickness of the "fluidized" layer, δ, is chosen to be equal to 0.03 cm, as discussed above. The current I is adjusted in order to reach the required total overvoltage.

The evolution of η_{fluid} and η_{C-F} versus distance r for various ρ values ($r_0 = 0.8$ cm and $T = 95$ °C) is presented in Fig. 14a. As expected, the overvoltage of the "fluidized" layer increases while that of the C–F decreases with increasing ρ values.

We have reported above that the electrochemical reaction takes place on a ring at the circumference of the electrode. Fig. 14b which presents the variation of the calculated current density versus distance r confirms this assumption: the j values are always small in the center of the electrode and increases towards the circumference. As a consequence, the size of the electrode should have a non negligible influence on the values of η_{fluid} and η_{C-F}. The variation of η_{fluid} and η_{C-F} versus distance r for several values of the radius r_0 ($\rho = 10\ \Omega$ cm) is presented in Fig. 15a. η_{fluid} decreases with decreasing r_0 values. At the same time, the current density (Fig. 15b) in the center of the electrode increase with decreasing r_0 values.

These results clearly show that the contribution of the "fluidized" layer must be taken into account for a good understanding of the fluorine evolution process.

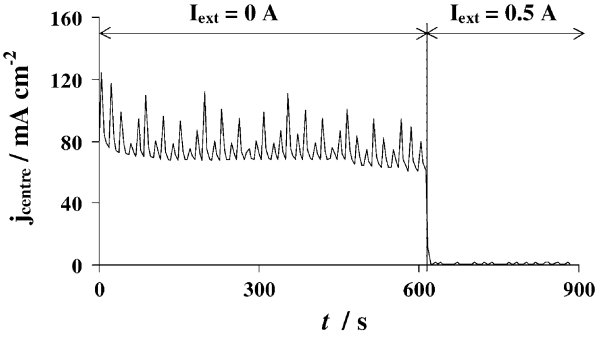

Fig. 13. Evolution of the total current density observed at the center of a ring-disk electrode disk, j_{center}, vs. time. I_{ext} is the current applied to the external electrode (ring).

3. Experimental details

For the experiments in molten KF–2HF at 95 °C (C_{H_2O} < 20 ppm or ≈600 ppm), a Cu/CuF_2 reference electrode (+0.4 V versus Pt–H_2) and a graphite auxiliary electrode were used; the latter was chosen to prevent any pollution of the melt by metal cations. The electrochemical cell is equipped with a Plexiglas window, which made visible inspection possible. Different materials were chosen for the electrochemical tests: non-graphitized carbon 205NG (Le Carbone Lorraine, France) and Ultra F (Johnson Matthey, GB), graphite G208 (Le Carbone Lorraine, France), vitreous carbon V25 (Le Carbone Lorraine, France), P2J industrial non-graphitized carbon for fluorine production (S.G.L., France) and HOPG (Union Carbide, USA, grade: ZYH).

Impedance measurements in KF–2HF were performed with a Solartron-Schlumberger 1255 impedance analyser coupled with an EG&G PAR model 273 potentiostat. The amplitude of the sinusoidal perturbation was 10 mV peak-to-peak; the frequency range was 1 MHz–1 Hz.

Impedance measurements in mercury were performed in the 13 MHz–5 Hz frequency range with a Hewlett-Packard 4192A frequency response analyser driven by a Hewlett-Packard 9816 microcomputer. The amplitude of the sinusoidal perturbation was 10 mV peak-to-peak. The cell used for these experiments is described in Fig. 16. For the study of the C/C–F/Hg structures, no potential was applied between the two electronic conductors (C and Hg). In that case, the

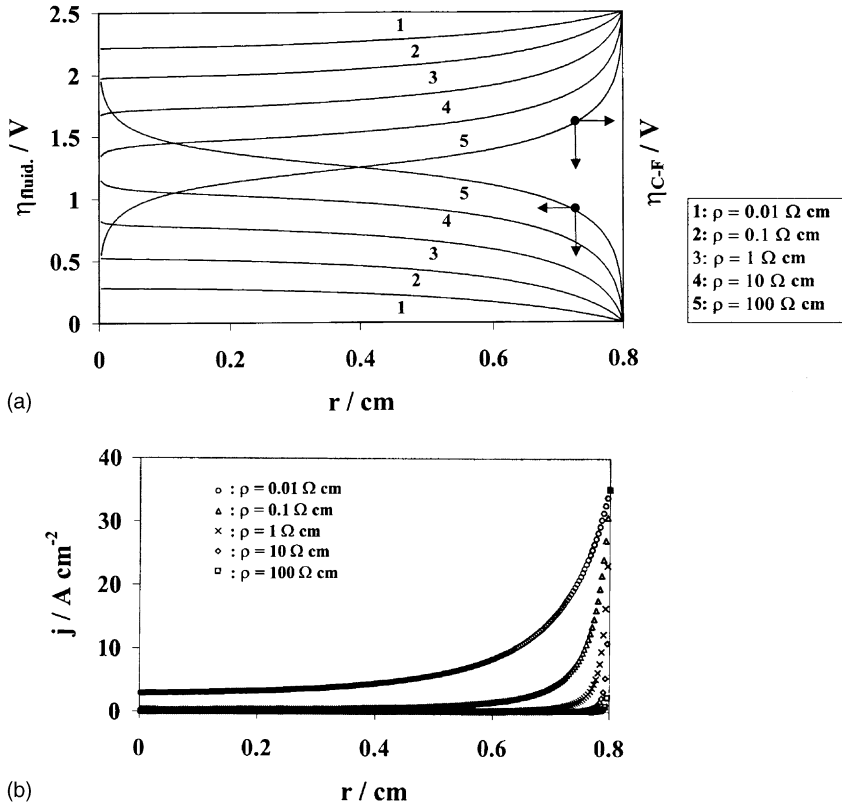

Fig. 14. Variation of (a) the overvoltage in the "fluidized" layer, η_{fluid}, in the C–F layer, η_{C-F}, and (b) the current density, j, vs. distance, r, for several values of the resistivity ρ of the "fluidized" layer, $\eta_T = 2.5$ V, $T = 95$ °C.

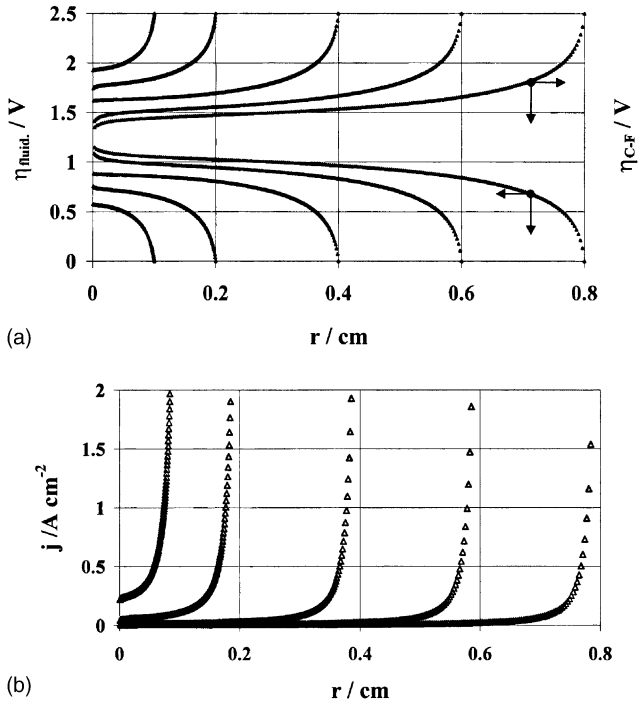

Fig. 15. Variation of (a) the overvoltage in the "fluidized" layer, η_{fluid}, in the C–F layer, η_{C-F}, and (b) the current density, j, vs. distance, r, for different electrode radius, r_0 (0.1, 0.2, 0.4, 0.6 and 0.8 cm), $\eta_T = 2.5$ V, $T = 95$ °C and $\rho = 10\ \Omega$ cm.

ionic conductivity of the surface film is not taken into account. Only the electronic properties of the surface films were studied. The experiments performed on these structures were made using purum 99.99999% mercury (Mercure Industries, France). The sample is put at the bottom of the cell. The height of the column of mercury is $h \approx 13$ cm for a good electric contact.

All the experimental data deduced from impedance measurements were analyzed with the Equivalent Circuit fitting program developed by B.A. Boukamp (University of Twente, The Netherlands).

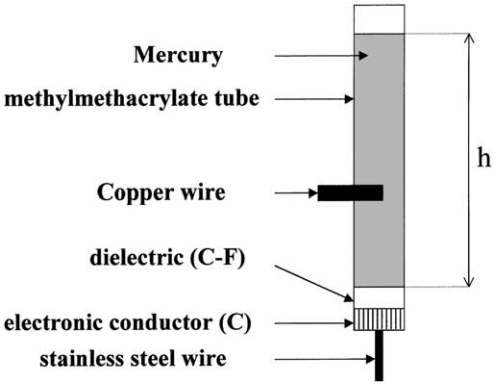

Fig. 16. Cell used for the impedance measurements in mercury with the C/C–F/Hg structures. (Reprinted from [25].)

The chronoamperograms were obtained with an EG&G PAR model 273 generator.

STM measurement was performed at first on pure HOPG. After cleavage, a HOPG sample was introduced into the electrochemical cell and passivated in KF–2HF at 6 V during 30 min. Then, the sample was rinsed with distilled water for eliminating traces of KF–2HF melt and treated at room temperature under vacuum for 1 day for removing traces of HF. The fluorinated sample was cleaved just before its study by STM. Nanoscope III and Pt/Ir tips from Digital Instruments were used for the STM analysis in air. The STM images were collected in constant-height mode with small bias voltage (20 mV) and an approach current (setpoint) of 4 or 5 nA.

4. Conclusion

The fluorine evolution reaction in molten KF–2HF was studied. The electronic properties of solid carbon–fluorine passivating film (denoted C–F) electrogenerated on the carbon anodes during electrolyis were investigated. Impedance measurements performed in presence of mercury with C/C–F/H structures have shown that the C–F films can be considered as electronic conductors and thus cannot constitute a high energy barrier for the electron transfer in electrochemical reactions. The study of the kinetics of $Fe^{III/II}$ redox couple on C/C–F structures has confirmed results obtained in mercury: the carbon anode covered by C–F film behaves like metallic platinum electrodes.

STM measurements were performed on HOPG fluorinated in KF–2HF or by chemical fluorination using fluorine gas. Whatever the preparation process, these experiments have shown that the C–F film is composed of conducting GIC and a small amount of graphite fluorides. In the case of electrochemical passivation in KF–2HF, the amount of graphite fluorides (CF_x) is strongly dependent on the water content in KF–2HF: the higher the water content, the higher the amount of insulating CF_x. Although, their contribution in term of electronic properties of the surface film is low, they have a great influence on the kinetics of the fluorine evolution reaction since they limit drastically the wettability of the electrode by KF–2HF. In the case of electrochemical fluorination in a dehydrated KF–2HF melt, the hexagonal symmetry of the HOPG is kept. By contrast, if the melt contains a high amount of water, the hexagonal symmetry of the starting material seems to be completely destroyed. In the same manner, a chemical fluorination of HOPG with F_2 gas leads to a strong distortion of the hexagonal structure of the starting material. The presence of CF_x at the surface explains why the approach of the tip cannot be done in some parts of the electrode since no current was detected, even for high bias.

In the case of an electrochemical fluorination in well dehydrated KF–2HF melt, two kinds of hexagonal symmetry have been revealed: in the first one, all the carbon atoms of the layer in the hexagonal ring are observed due to the intercalation of HF_2^- species which increases the distance between two carbon sheets; in the second one, the same hexagonal symmetry as that of HOPG was observed with a periodicity of 2.44 nm. The overlap of the electronic densities between two neighboring fluorine atoms two carbon atoms was observed.

The C–F film is mainly composed of conducting compounds belonging to the graphite intercalation compounds (GICs) family in which the C–F bonds are ionic and/or semi-ionic. Therefore, the fluorine evolution mechanism does not obey to a mechanism involving electron tunneling through a passive film: the electron can be easily transferred from the electrolyte to the electrode. Nevertheless, traces of insulating CF_x were pointed out by scanning tunneling microscopy (STM).

During fluorine evolution, the electrode surface is almost completely covered by bubbles. Nevertheless, high value of current intensity can flow at the electrode/electrolyte interface. To explain such phenomenon, the influence of mass transfer on the kinetics of the FER was studied in KF–2HF mainly by impedance spectroscopy with a rotating disk electrode facing the bottom of the electrochemical cell. To give a good interpretation of the results obtained, a new model for the representation of the electrode/electrolyte interface has been proposed including the presence of an intermediate layer between the electrode surface and the gaseous film. This intermediate layer is supposed to be composed of a mixture of liquid KF–2HF and fluorine bubbles. This layer gives rise to a contribution at very high frequency. Its characteristic frequency is about 200 kHz; the associated resistance is about $3\ \Omega\ cm^2$ and is constant whatever the ω and E values.

Therefore, the kinetics rate of the FER is governed both by mass transfer and charge transfer. The total anodic overvoltage, η_T, observed during the fluorine evolution process results not only from the overvoltage due to solid C–F surface film (η_{C-F}), but also from the overvoltage due to the ''fluidized'' layer (η_{fluid}). Numerical calculations were performed to determine each contribution versus the electrode radius, r_0, and the resistivity, ρ, of the ''fluidized'' layer. These results have confirmed the fact that the existence of the ''fluidized'' layer cannot be neglected for a good understanding of the fluorine evolution process. For instance, η_{fluid} and η_{C-F} are equal to 1 and 1.5 V, respectively for $\rho = 10\ \Omega$ cm, $T = 95\ ^\circ C$ and $r_0 = 0.8$ cm.

Acknowledgements

The author would like to thank to Prof. D. Devilliers, Drs. F. Lantelme, S. Durand-Vidal, F. Nicolas, J.-P. Caire, C. Belhomme, C. Hinnen, P. Marcus, M. Combel and M. Vogler for helpful and fruitful discussions and assistance in the experimental work. Grateful acknowledgments are made to the Comurhex-Cogema Company (Pierrelatte, France) for their joint-support of this research project.

References

[1] A.J. Rudge, Production of elemental fluorine by electrolysis, in: A. T. Kuhn (Ed.), Industrial Electrochemical Process, Elsevier, Amsterdam, 1971, Chapter 1, pp. 1–69.

[2] H. Groult, D. Devilliers, M. Vogler, Trends in the fluorine preparation process, in: Proceedings of the Current Topics in Electrochemistry, vol. 4, Research trends, Poojupura, Trivandrum, India, 1997, pp. 23–39.

[3] D. Devilliers, M. Chemla, Carbon anode reaction in fluorine production, in: T. Nakajima (Ed.), Fluorine-Carbon and Fluoride-Carbon Materials, Marcel Dekker, New York, 1995, Chapter 8, pp. 283–331.

[4] D. Devilliers, F. Lantelme, M. Chemla, J. Chem. Phys. 76 (1979) 428–432.

[5] O.R. Brown, Electrochim. Acta 25 (1980) 367–368.

[6] T. Nakajima, Synthesis, Structure and physicochemical properties of fluorine-graphite intercalation compounds, in: T. Nakajima (Ed.), Fluorine-Carbon and Fluoride-Carbon Materials, Marcel Dekker, New York, 1995, Chapter 1, pp. 1–31.

[7] H. Imoto, T. Nakajima, N. Watanabe, Bull. Chem. Soc. Jpn. 48 (1975) 1633–1634.

[8] L. Bai, B.E. Conway, J. Appl. Electrochem. 18 (1988) 839–848.

[9] N. Watanabe, T. Nakajima, H. Touhara, Anode Effect in Molten Fluorides, Graphite Fluorides, vol. 8, Elsevier, Amsterdam, 1988, Chapter 1, pp. 1–22.

[10] D.M. Novak, P.T. Hough, J. Electroanal. Chem. 144 (1983) 121–133.

[11] O.R. Brown, B.M. Ikeda, M.J. Wilmott, Electrochim. Acta 32 (1987) 1163–1171.

[12] H. Groult, D. Devilliers, M. Vogler, C. Hinnen, P. Marcus, F. Nicolas, Electrochim. Acta 38 (1993) 2413–2421.

[13] L. Bai, B.E. Conway, J. Appl. Electrochem. 20 (1990) 916–924.

[14] P. Cadman, J.D. Scott, J.M. Thomas, Carbon 15 (1977) 75–86.

[15] M. Chemla, D. Devilliers, J. Electrochem. Soc. 136 (1989) 87–91.

[16] T. Nakajima, T. Ogawa, N. Watanabe, J. Electrochem. Soc. 134 (1987) 8–11.

[17] D. Devilliers, B. Teisseyre, M. Chemla, Electrochim. Acta 35 (1990) 153–162.

[18] P.T. Hough, D.M. Novak-Antoniou, US Patent 4,602,985 (1986).

[19] N. Watanabe, M. Inoue, S. Yoshizawa, J. Electrochem. Soc. Jpn. 31 (1963) 113–117.

[20] T. Tojo, J. Hiraiwa, M. Dohi, Y.-B. Chong, N. Watanabe, J. Fluorine Chem. 54 (1991) 136.

[21] T. Tojo, Metal fluoride-impregnated carbon electrode for fluorine production, in: T. Nakajima (Ed.), Fluorine-Carbon and Fluoride-Carbon Materials, Marcel Dekker, New York, 1995, Chapter 9, pp. 333–354.

[22] Asahi Glass Co., JP-Kokai Patent 58,81,981 (1983).

[23] O.R. Brown, M.J. Wilmott, European Patent 255,225 (1988).

[24] W.V. Childs, G.L. Bauer, J. Electrochem. Soc. 142 (1995) 2286.

[25] H. Groult, D. Devilliers, S. Durand-Vidal, F. Nicolas, M. Combel, Electrochim. Acta 44 (1999) 2793–2803.

[26] H. Groult, F. Lantelme, J. Electrochem. Soc. 148 (2001) E13–E18.

[27] H. Groult, D. Devilliers, F. Lantelme, J.-P. Caire, F. Nicolas, M. Combel, J. Electrochem. Soc. 149 (2002) E485–E492.

[28] L.J.J. Janssen, J.G. Hoogland, Electrochim. Acta 15 (1970) 1013–1023.

[29] H. Vogt, in: E. Yeager, J.O'M. Bockris, B.E. Conway (Eds.), Comprehensive Treatise of Electrochemistry, vol. 6, Plenum Press, New York, 1983, pp. 445–489.

[30] J.W. Schultze, L. Elfenthal, J. Electroanal. Chem. 204 (1986) 153–171.

[31] O. Kerrec, Thesis, Paris, France, 1992.

[32] R. Wiesendanger, D. Anselmetti, STM on layered materials, in: H.-J. Güntherodt, R. Wiesendanger (Eds.), Scanning Tunnelling Microscopy, vol. 1, Springer, Berlin, 1992, pp. 131–179.

[33] C. Daulan, J.C. Roux, H. Saadaoui, S. Flandrois, A. Tressaud, K. Amine, T. Nakajima, J. Solid State Chem. 107 (1993) 27–33.

[34] T. Nakajima, N. Watanabe, Physicochemical Properties of Fluorine-Graphite Intercalation Compounds, Graphite Fluorides and Carbon-Fluorine Compounds, CRC Press, Boca Raton, 1991, Chapter 7, pp. 155–171.

[35] H. Groult, D. Devilliers, M. Vogler, P. Marcus, F. Nicolas, J. Electrochem. Soc. 144 (1997) 3361–3366.

[36] T. Nakajima, M. Touma, J. Fluorine Chem. 57 (1992) 83–91.

[37] J. Barber, S. Morin, B.E. Conway, J. Electroanal. Chem. 446 (1998) 125–138.

[38] N. Watanabe, M. Ishii, S. Yoshizawa, J. Electrochem. Soc. Jpn. 29 (1961) 177–186.

[39] H. Roustan, Thesis, Grenoble, France, 1998.

[40] H. Groult, S. Durand-Vidal, D. Devilliers, F. Lantelme, Kinetics of fluorine evolution reaction on carbon anodes: influence of the surface C–F films, J. Fluorine Chem. 107 (2001) 247–254.